General Features of Squall Lines in East China

ZHIYONG MENG, DACHUN YAN, AND YUNJI ZHANG

Laboratory for Climate and Ocean–Atmosphere Studies, Department of Atmospheric and Oceanic Sciences, School of Physics, Peking University, Beijing, China

(Manuscript received 27 July 2012, in final form 4 November 2012)

ABSTRACT

Based on mosaics of composite radar reflectivity patterns during the 2-yr period of 2008–09, a total of 96 squall lines were identified in east China with a maximum frequency of occurrence in north China near the boundaries between Shandong, Henan, Anhui, and Jiangsu Provinces. The squall lines form from March to October with a peak in July. Their diurnal variation shows a major peak in the early evening and two minor peaks in the early morning and early afternoon. The time between squall-line formation and the first echo is about 4.8 h. The squall lines have a dominant southwest–northeast orientation, an eastward motion at a speed of 14.4 m s^{-1}, a maximum length of 243 km, a maximum intensity of 58–63 dBZ, and a duration of 4.7 h on average. The squall lines commonly form in a broken-line mode, display a trailing-stratiform pattern, and dissipate in a reversed broken-line mode. Composite rawinsonde analyses show that squall lines in mid-latitude east China tend to form in a moister environment with comparable background instability, and weaker vertical shear relative to their U.S. counterparts. The rawinsondes were also composited with respect to different formation and organizational modes. The environmental flows of the squall lines in the area with high frequency of formation were classified into six synoptic weather patterns: pre–short trough, pre–long trough, cold vortex, subtropical high, tropical cyclone (TC), and posttrough. About one-third of the squall lines form in the dominant pre-short-trough pattern. Favorable conditions of various patterns were examined in terms of moisture supply, instability, vertical wind shear, low-level jet, etc.

1. Introduction

Squall lines are linear or quasi-linear mesoscale convective systems (MCSs) that can produce heavy rains, damaging winds, hail, and sometimes even tornadoes. A squall line is defined as ''a line of active thunderstorms, either continuous or with breaks, including contiguous precipitation areas resulting from the existence of the thunderstorms (Glickman 2000).'' Common radar signatures of squall lines are composed of a leading edge of a convective rainband with a width of several tens of kilometers and a length of several hundreds of kilometers followed by a large area of stratiform rainfall. There is usually an apparent cold pool close to the surface in the convective area with its leading edge known as the gust front. Strong updrafts appear in front of the cold pool while downdrafts are found in the convective area with moderate upward and downward motions in the stratiform area. Abrupt changes of surface pressure, temperature, wind, etc. are usually seen across the gust front, where disastrous weathers tend to occur. For example, strong surface winds are partly associated with the large surface pressure gradient between the prelow in front of the gust front and the storm high in the cold pool. Squall lines usually form in an environment with moderate to high instability and low-level vertical shear. They are commonly initiated and maintained by the lifting in the area between the baroclinically generated horizontal vorticity associated with the cold pool and the horizontal vorticity with the opposite sense of rotation associated with ambient vertical wind shear known as Rotunno–Klemp–Weisman (RKW) theory (Rotunno et al. 1988). Squall lines may take on different features such as morphologies and dominant disasters in regions with different environmental conditions (Chen and Chou 1993; Meng and Zhang 2012, hereafter MZ12). Operational forecasts of MCSs, especially squall lines, have been important yet difficult due to their rapid

Corresponding author address: Dr. Zhiyong Meng, Laboratory for Climate and Ocean–Atmosphere Studies, Dept. of Atmospheric and Oceanic Sciences, School of Physics, Peking University, 209 Chengfu Rd., Haidian District, Beijing 100871, China.
E-mail: zymeng@pku.edu.cn

DOI: 10.1175/MWR-D-12-00208.1

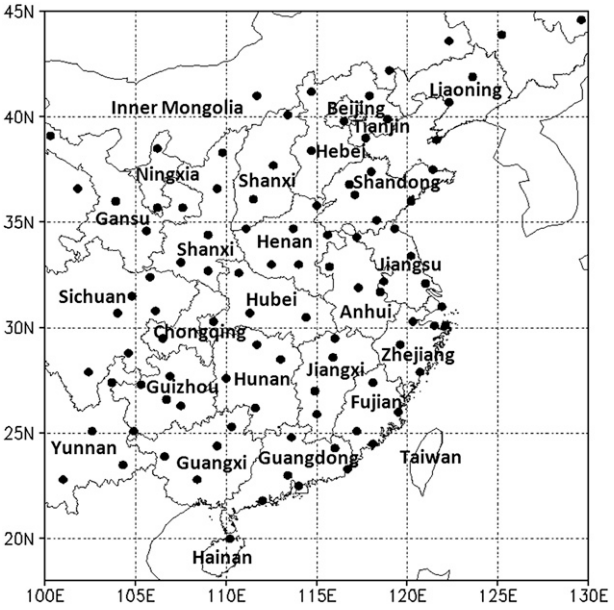

FIG. 1. Map of east China with the names of related provinces and the locations of operational radar stations (black dots).

development, fast movement, and severe disastrous weather. A good knowledge of the general characteristics of squall lines such as the spatial and temporal distributions, morphology, and formation environment can obviously aid forecasters in making short-time forecasts.

Squall lines are commonly responsible for severe weather in the United States, where their attributes have been well documented (e.g., Bluestein and Jain 1985; Wyss and Emanuel 1988; Houze et al. 1990; Geerts 1998; Parker and Johnson 2000; Jirak et al. 2003). Squall lines are also commonly responsible for severe weather in China. For example, a squall line formed in Henan Province (refer to its location in Fig. 1 at around 34°N, 114°E) during June 2009, which brought a strong wind of 29.1 m s^{-1} and resulted in 27 deaths (Zhang et al. 2012). Previous studies examined features of subtropical squall lines in Taiwan Strait (Chen and Chou 1993) and those preceding landfalling tropical cyclones (TCs) in China (MZ12). These studies showed that subtropical and pre-TC squall lines in China tend to have a shorter maximum length, a similar speed of movement, a longer (shorter) life span for the subtropical (pre-TC) squall lines, a formation environment with similar instability, lower vertical shear, and are more humid relative to their counterparts in the United States. However, the general features of squall lines in large areas of China, as well as their climatological features and differences from squall lines in other areas such as the United States, are unknown.

Radar mosaics have been widely used in statistical studies of squall lines in the United States (Wyss and Emanuel 1988; Geerts 1998; Parker and Johnson 2000). The radar network in east China (Fig. 1) has become dense enough to examine general features of squall lines. This paper is aimed at documenting basic features of squall lines in east China including their temporal and spatial distributions, length, intensity, duration, orientation, movement, formation, dissipation, and organizational modes, as well as environmental features based on two available full-year composite radar reflectivity mosaics in 2008 and 2009. Comparisons between the features of squall lines in east China and those in the United States will also be conducted. This work is expected to have important implications for real-time squall-line forecasting in China and contribute to the general knowledge of squall lines in different climate regimes around the globe.

Section 2 describes the data and methodology. The radar features of the squall lines are described in section 3. Section 4 presents environmental features of the squall lines in their high-frequency regions. Section 5 shows how weaker criteria in defining squall lines may affect their statistical features, and a summary is given in section 6.

2. Data and methodology

This survey was based on the digital mosaics of composite Doppler radar reflectivity (the horizontal distribution of vertical maximum radar reflectivity) in 2008 and 2009 with a time interval of 20 (10) min before (after) 22 September 2008, 4 km $\times$ 4 km horizontal resolution, and 85% of time coverage. The radar mosaics are operationally produced by the China Meteorological Administration based on a network of Chinese next-generation weather radars (their locations are given by the black dots in Fig. 1). The radars in east China and coastal areas are S-band radars, while those in northwest and northeast China are C-band radars. The S-band radars used in China are similar to Weather Surveillance Radar-1988 Dopplers (WSR-88Ds) in the United States in both their hardware and software (Zhu and Zhu 2004). This is the same dataset as that used in MZ12.

There have been several different criteria used in defining a squall line in the literature, as listed in Table 1. MZ12 used criteria similar to those in Parker and Johnson (2000): 1) a contiguous or quasi-contiguous band of 40-dBZ reflectivity extends at least 100 km and lasts at least 3 h and 2) the 40-dBZ region has a linear or quasi-linear shape with an apparent common leading edge. The same criteria were used in this work except that the 40-dBZ band was required to be strictly contiguous. This

TABLE 1. Several of the criteria used to define linear MCSs (squall lines) in the literature in addition to this work.

	Chen and Chou (1993)	Geerts (1998)	Parker and Johnson (2000)	Meng and Zhang (2012)	Squall line in this work
Time and coverage	May–Jun 1987	May 1994–Apr 1995	May of 1996 and 1997	Jun 2007–Dec 2009	2008–09
Area	Taiwan and Taiwan Strait	Southeast United States	Central United States	Pre-TC squall lines in east China	Squall lines in east China
No. of MCSs	6	187	88	17	96
Criteria	(a) Band of larger than 12 dBZ ≥150 km and lasting ≥5 h (b) LWR of larger than 36-dBZ band ≥3:1 at mature	a) Band of larger than 20 dBZ ≥100 km and lasting ≥4 h (b) Band of larger than 40 dBZ lasting ≥2 h with an LWR ≥ 5:1	(a) Band of contiguous or quasi-contiguous larger than 40 dBZ ≥100 km and lasting ≥3 h (b) Linear or quasi-linear convective area sharing a common leading edge	As in Parker and Johnson (2000); "quasi contiguous" was interpreted as that 40-dBZ band can be noncontiguous but the 35-dBZ band in which the 40-dBZ convection is embedded in has to be strictly contiguous	As in Parker and Johnson (2000), but here the 40-dBZ convection is strictly contiguous

additional requirement makes the sample identification more objective and focuses on stronger squall lines. The radar traits of thus-determined squall lines are defined in Table 2, including the formation time, dissipation time, duration, maximum length, orientation, speed of movement, intensity, formation mode, and organizational mode.

3. General features of squall lines in east China

With the criteria defined in section 2, a total of 96 squall lines were identified. The spatial distribution of their formation frequency is shown in Fig. 2a. The largest frequency of formation is evident around 35°N, 117°E near the boundaries between Anhui, Henan, Shandong, and Jiangsu Provinces (area B in Fig. 2a, the names of the provinces are given in Fig. 1). The second largest frequency of formation appears in southern Hebei Province (area A). Two other minor maxima lie in southern Fujian (area C) and southwestern Guangdong Provinces (area D). One interesting signature is that most squall lines form in flat areas. This feature can be due to the observational limit and beam blockage of radars in hilly areas on the one hand, and the tendency of squall lines to form in relatively flat areas on the other, similar to the distribution of the warm season rainfall in north China based on satellite-derived precipitation (He and Zhang 2010; Bao et al. 2011).

About 87% of the squall lines have an eastward component of movement (Figs. 2b–e). The dominant eastward movement of the squall lines is especially apparent in higher latitudes. Less eastward movement is observed in lower latitudes in autumn likely due to those squall lines associated with the subtropical high and TCs, which will be discussed in detail in section 4. The eastward motion is clearly shown in the mean tracks during different seasons (Fig. 2e). It also shows that the mean formation position of the squall lines in east China first appears in spring around 27°N, shifts northward to about 32°N in summer, then moves southward again to about 26°N in autumn.

An apparent seasonal variation of the frequency of formation of the squall lines is also observed in Figs. 2b–e and 3a. A total of 18 (about 19%) squall lines formed in spring (Figs. 2b and 3a). Nearly 74% of the squall lines occur in summer with a peak in July (Figs. 2c and 3a), most of which appear in north China near areas A and B (Fig. 2c). Only seven squall lines formed in autumn and they are all to the south of 35°N (Figs. 2d and 3a). The major formation peak in July has also been observed in previous surveys of MCSs in the United States (Geerts 1998; Jirak et al. 2003). There are three peaks of squall-line formation in diurnal variation with

TABLE 2. Definitions of various radar traits of the squall lines in the present work.

Formation time	When the squall line threshold is first met
Dissipation time	Time when the squall-line threshold is continuously last met for more than 3 h after its formation
Duration	Period during which the squall-line threshold is continuously met
Max length	The length of the maximum straight long axis of a contiguous 40-dBZ reflectivity band
Orientation	The dominant orientation during the life span of a squall line using the azimuthal angle of a straight line connecting the two endpoints of the 40-dBZ band [similar to Parker and Johnson (2000)]
Speed of movement	The length of a straight line connecting the midpoints of the hourly isochrones at the leading edge of the quasi-linear 40-dBZ band during the lifetime divided by the lifetime (similar to Wyss and Emanuel 1988; Parker and Johnson 2000)
Intensity	The maximum value of the radar composite reflectivity during the lifetime
Formation mode	The dominant mode used to represent the formation process of a squall line, including broken line, back building, broken areal, and embedded areal, as defined by Bluestein and Jain (1985)
Organizational mode	The dominant juxtaposition of stratiform and convective rainfall, including leading stratiform, trailing stratiform, and parallel stratiform, as defined by Parker and Johnson (2000)

a major peak at 1800–2100 local standard time (LST = UTC + 8) and two minor peaks at 0300–0600 and 1200–1500 LST (Fig. 3b). The early morning and late-evening peaks are similar to those of the linear MCSs in the United States (Parker and Johnson 2000). The major peak found in the late evening was also observed by Jirak et al. (2003) in their survey of MCSs in the central United States. Geerts (1998) found that the major peak of MCSs in the southeast United States is in the late afternoon. The peak in the early afternoon has not been documented in the literature.

The diurnal variation is closely related to the latitudes of the squall lines. The squall lines that form to the south of 30°N exhibit different diurnal features from those that form to the north of 30°N (Fig. 3c). The peak of 1800–2100 LST is observed for both areas. However, the early morning peak of 0300–0600 LST is mainly attributed to the squall lines to the south of 30°N, while the early afternoon peak of 1200–1500 LST is mainly attributed to the squall lines to the north of 30°N. This result indicates that the possibility of squall-line formation during 1200–1500 LST increases at higher latitudes.

Convective-initiation features of the squall lines were also examined. Each squall line was traced back to the appearance of its first convective echo of 40 dBZ (the dotted part of the squall-line tracks in Figs. 2b–e). The geographical distribution of these first echoes as shown in Fig. 2f demonstrates that the high frequency of occurrence of first radar echoes clearly shifts to the west north of 26°N and to the east south of 26°N relative to the formation positions of the squall lines. The distribution of the time between the appearances of the first echoes and the formation of the squall lines is plotted in Fig. 3d. The result shows that most squall lines take 1–5 h to organize into a squall line with an average time of 4.8 h, which is similar to the mean life span of the squall lines. The time between the first echoes and the formation of the squall lines seems to be insensitive to their latitudes (Fig. 3f). The average time lag is 4.7 h (4.9 h) to the south (north) of 30°N. The diurnal variation of the frequency of occurrence of the first radar echoes has a single peak near 0900–1200 LST (Fig. 3b), which is about 9 h earlier than the major peak (1800–2100 LST) of the squall-line formation time.

The different features of the diurnal variation of the squall lines at their formation times between areas to the north and south of 30°N as discussed before are likely due to the differences in the diurnal variation features of

→

FIG. 2. (a) The geographical distribution of the frequency of squall-line formation (blue shading). Darker shading denotes higher frequency. The numbers indicate the frequency of the squall lines in the corresponding data square that spans a 2° × 2° area and represent the number of times that the centroids of squall lines lie within the grid square at their formation times. Capital letters A–D in (a) denote various high-frequency areas. Squall line tracks are shown for (b) March–May, (c) June–August, and (d) September–October. (e) The average tracks of spring [those in (b)], summer [those in (c)], and autumn [those in (d)]. The dotted (solid) lines in (b)–(e) denote the tracks before (after) the formation of the squall lines with the open (filled) circles denoting the centroids of the first radar echo (squall line at formation times). The squall-line tracks in a month are set in the same color as that for the month in the panel captions. (f) The geographical distribution of the frequency of the first radar echoes of 40 dBZ (shaded in blue). The gray shading in (a) and (f) denotes the terrain height (every 200 m until 1600 m). The gray shading in (b)–(d) denotes the frequency of squall-line formation during the corresponding periods. The gray shading in (e) denotes the frequency of squall-line formation, which is the same as the blue shading in (a).

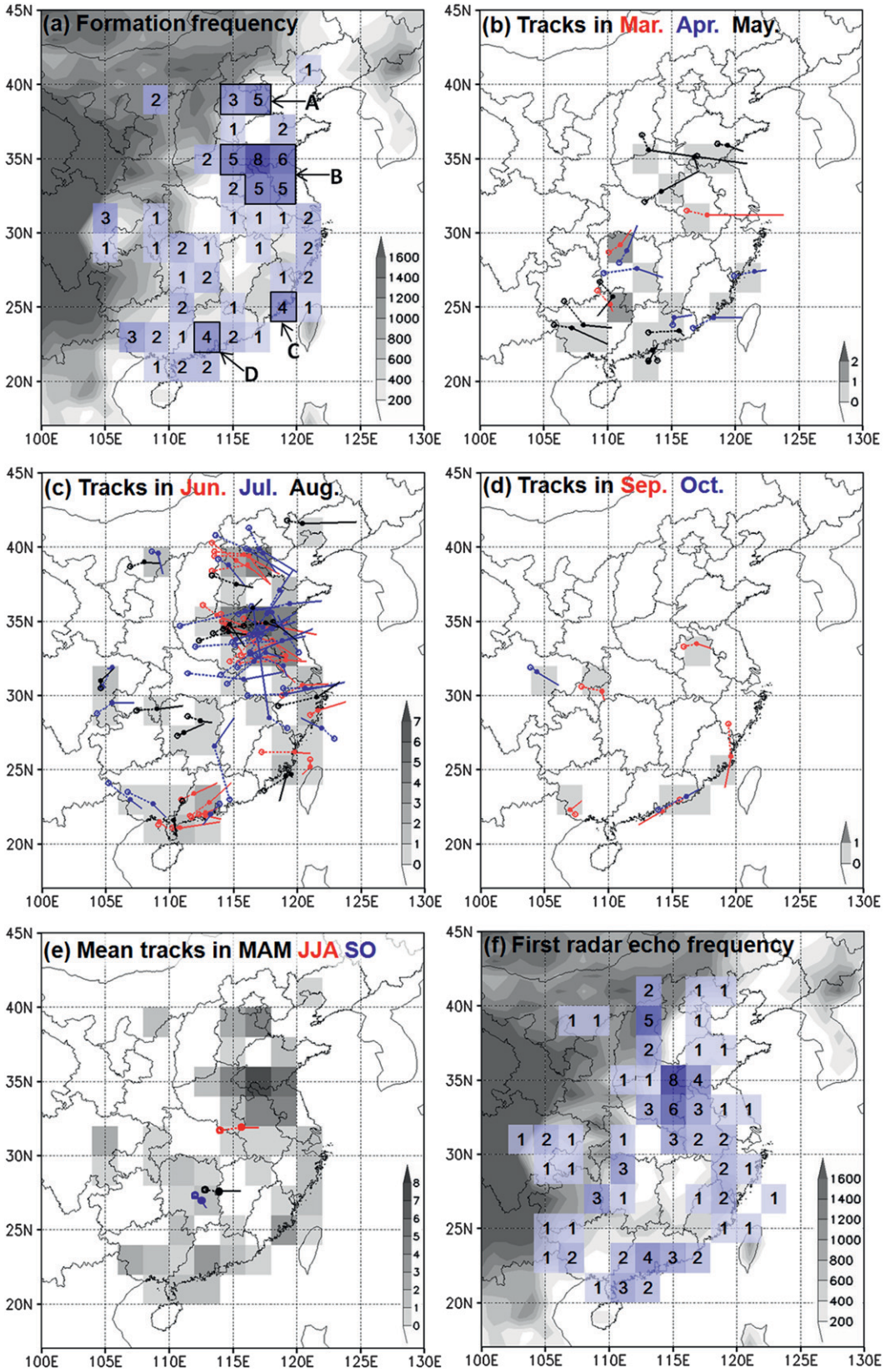
(a) Formation frequency
A
B
C
D
(b) Tracks in Mar. Apr. May.
(c) Tracks in Jun. Jul. Aug.
(d) Tracks in Sep. Oct.
(e) Mean tracks in MAM JJA SO
(f) First radar echo frequency
45N
40N
35N
30N
25N
20N
100E
105E
110E
115E
120E
125E
130E

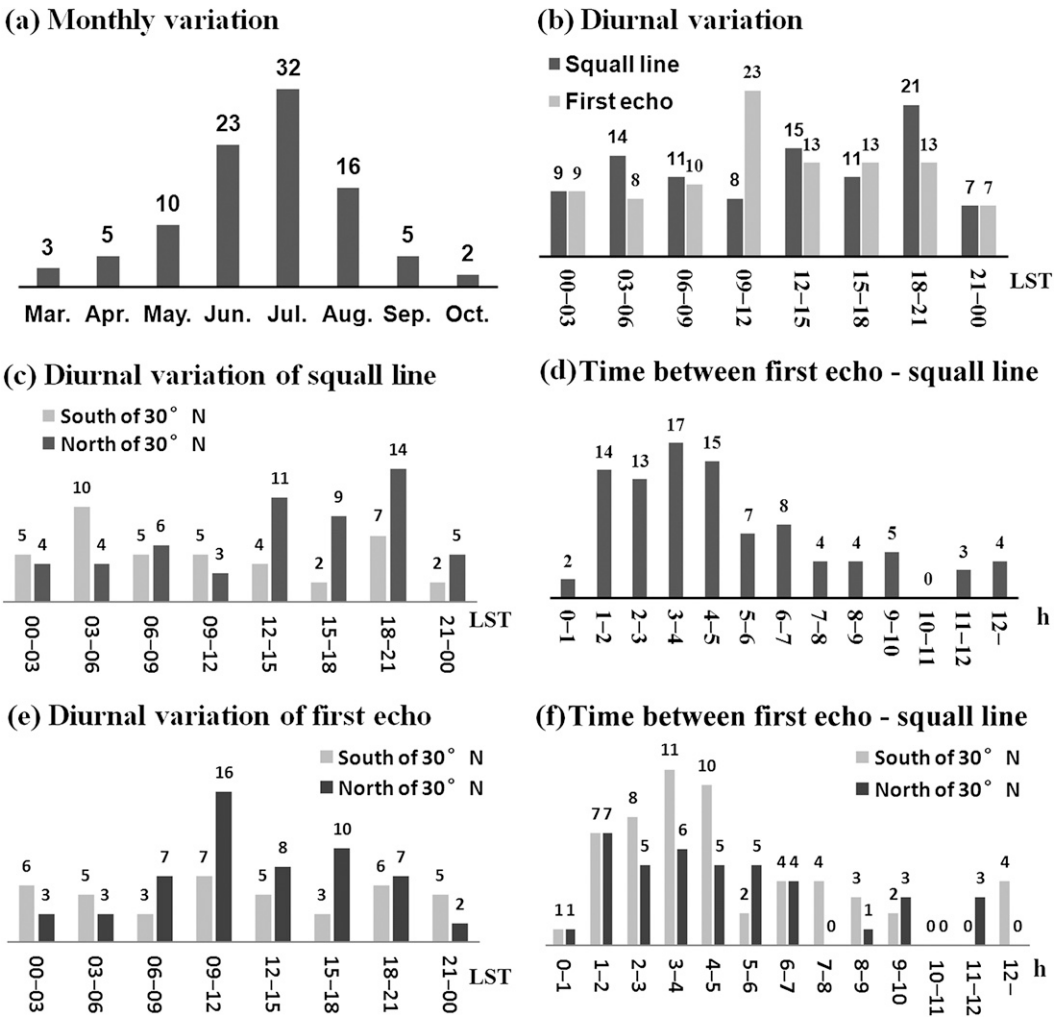

FIG. 3. The (a) monthly and (b) diurnal variations of the frequency of squall-line formation (dark gray) as well as first convective echoes (light gray). Also plotted are (c) the diurnal variations of the frequency of squall-line formation and (e) first echoes to the south (light gray) and north (dark gray) of 30°N. The frequency of the time between first echo and the formation of the corresponding squall line (d) for all of the squall lines and (f) for those to the south (light gray) and north (dark gray) of 30°N, respectively.

the first echoes (Fig. 3e). The early morning peak that is mainly attributed to the squall lines to the south of 30°N as shown in Fig. 3c is clearly associated with the early morning peak of the first echoes in the same area, while the early afternoon peak that is mainly attributed to the squall lines to the north of 30°N as shown in Fig. 3c is apparently associated with the noon peak of the first echoes in the same area. Considering the similar time between first echo and squall-line formation in the areas to the north and south of 30°N (Fig. 3f), this result indicates that the diurnal variation of the frequency of formation of the squall lines is mainly determined by the diurnal variation of their first echoes.

Squall lines may form from their first radar echoes in various fashions. As proposed by Bluestein and Jain (1985), formation modes of squall lines can be classified into broken line (BL, new cells develop between old cells and merge with them to form a contiguous or quasi-contiguous line), back building (BB, new cells form serially in the upstream of the original cells and merge with them and form a line), broken areal (BA, a convective band forms among scattered cells), and embedded areal (EA, a convective band forms in a widespread stratiform region). Jirak et al. (2003) extended the classification of Bluestein and Jain (1985) to a more comprehensive three-level scheme based on the presence of stratiform precipitation (including embedded and not embedded), arrangement of convective cells (including line, areal, and combination), and interaction of convective clusters (including isolated, merger, and nonmerger), which

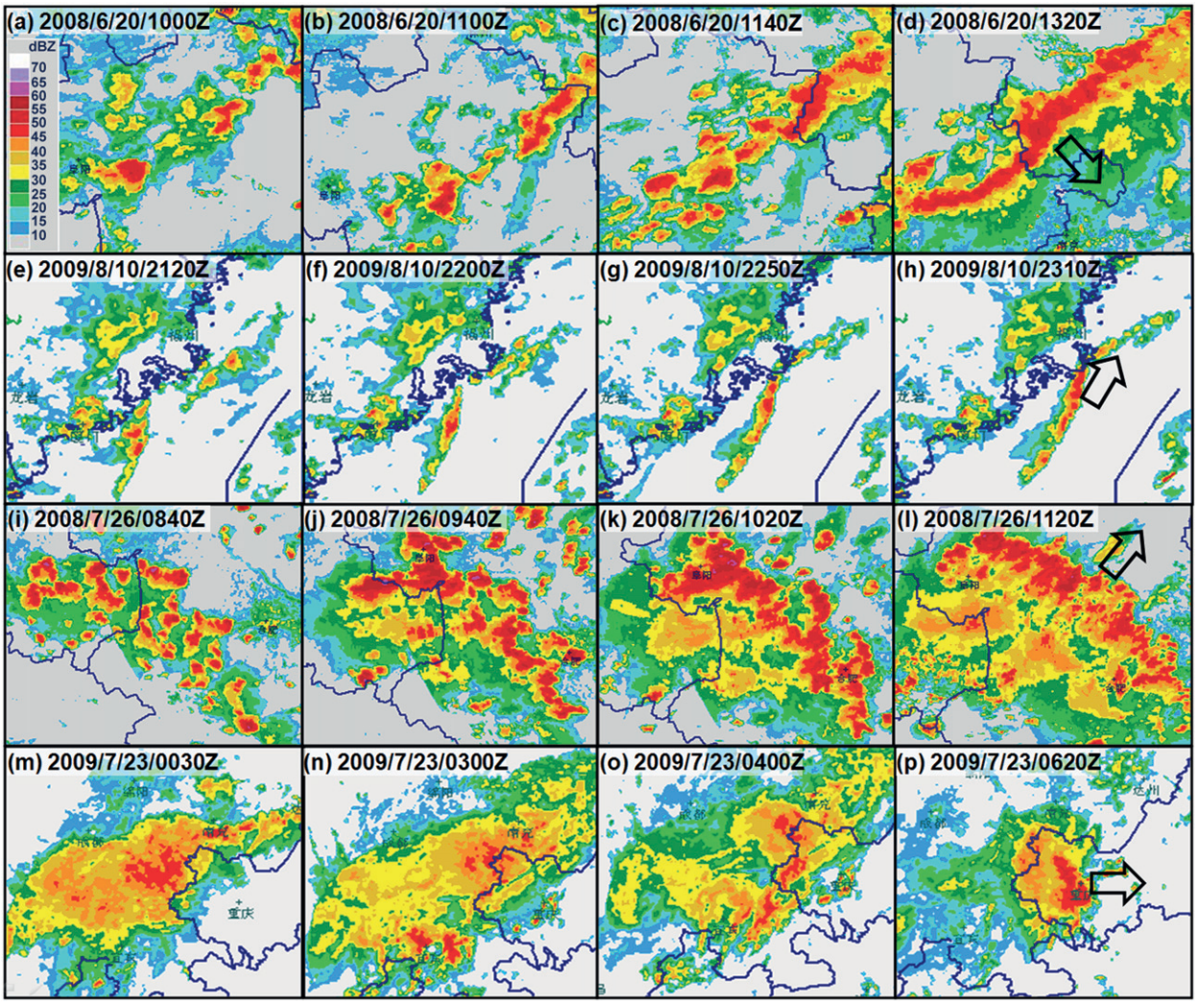

FIG. 4. The composite radar reflectivity (shading in dBZ) of four examples of the squall lines with different formation and organizational modes. Shown are patterns for (a)–(d) leading stratiform and broken line, (e)–(h) parallel stratiform and back building, (i)–(l) trailing stratiform and broken areal, and (m)–(p) trailing stratiform and embedded areal. The open arrow in the last panel of each case denotes the direction of movement of the squall line during the period shown. The geography is fixed in row 2, but repositioned on the squall line in rows 1, 3, and 4.

leads to a total of 17 categories. To make the classification easier to apply, the present work follows the widely used classification scheme of Bluestein and Jain (1985). The result shows that 37 (38%) squall lines form by BL (e.g., Figs. 4a–d), 21 (22%) by BB (e.g., Figs. 4e–h), 18 (19%) by BA (e.g., Figs. 4i–l), and 20 (21%) by EA (e.g., Figs. 4m–p). The dominant BL formation mode is consistent with the results of MZ12 but slightly different from those for squall lines in Oklahoma, where the frequencies of the BL and BB modes are comparable (Bluestein and Jain 1985). The percentage of the squall lines that form by the EA mode is apparently larger than that of the pre-TC squall lines and squall lines in Oklahoma and also MCSs in the central United States (Jirak et al. 2003). The EA squall lines form mainly in June–August to the south of 35°N. This may be associated with the mei-yu front and the high moisture environment of China, as will be demonstrated in section 4.

Besides the formation mode, the organizational mode of the squall lines in east China was also explored. The dominant (62%) organizational mode is trailing stratiform (TS, e.g., Figs. 4l,p) as defined in Parker and Johnson (2000), in which stratiform rainfall is located behind convective rainfall with respect to the direction of movement of the squall line. In the 96 cases, 25 cases (26%) take on a parallel stratiform mode (PS, in which stratiform rainfall is parallel to convective rainfall, e.g., Fig. 4h), and 11 cases (12%) take on a leading stratiform

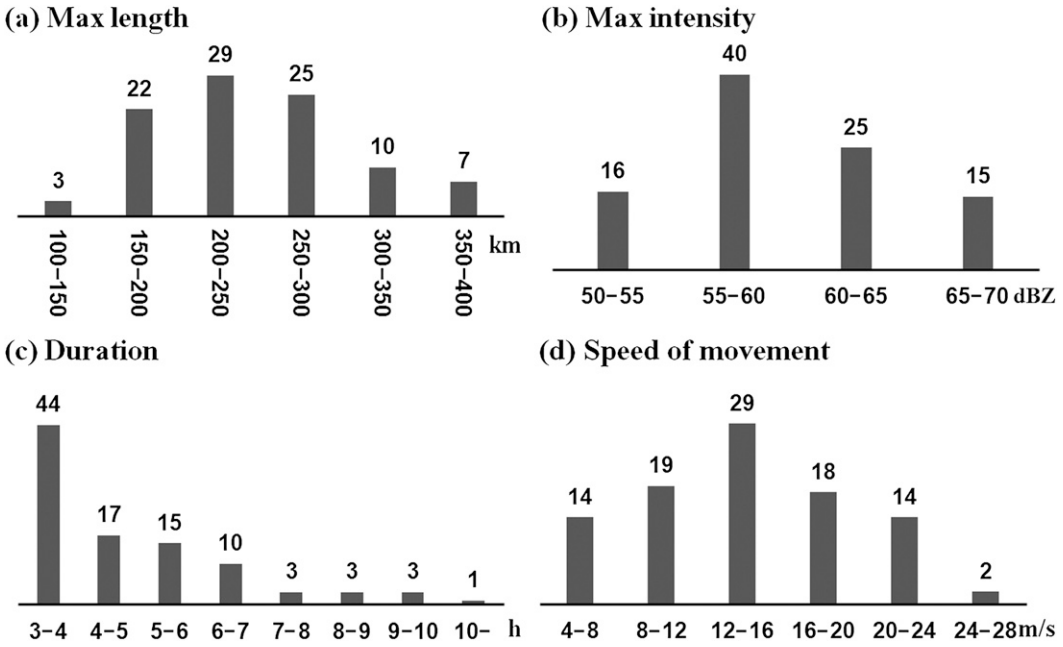

FIG. 5. The frequency of the squall lines with respect to various radar traits including (a) maximum length, (b) maximum intensity in terms of composite radar reflectivity, (c) duration, and (d) speed of movement.

mode (LS, in which stratiform rainfall is observed ahead of convective rainfall with respect to the direction of movement of the squall line, e.g., Fig. 4d). The percentages of the squall lines with different organizational modes are consistent with the results of squall lines in the central United States [60% for TS, 20% for LS, and 20% for PS; Parker and Johnson (2000)].

Various radar traits of these squall lines were then explored (Fig. 5). The maximum length of the squall lines ranges from 100 to 400 km with an average of 243 km (Fig. 5a). The squall lines have an average maximum intensity of 58–63 dBZ with 40% lying in the 55–60-dBZ range (Fig. 5b). Their life spans range from 3 to 13.5 h with an average of 4.7 h and a clearly left-skewed distribution (Fig. 5c). The frequency of the speed of movement of the squall lines peaks at 12–16 m s^{-1}. The average and largest speeds of movement are 14.4 and 25.6 m s^{-1}, respectively (Fig. 5c). About 43%, 22%, 19%, and 16% of the squall lines are oriented in southwest–northeast, north–south, west–east, and southeast–northwest directions, respectively.

Unlike formation modes, dissipation modes of squall lines have not been paid much attention in the literature. The dissipation modes of squall lines in east China in 2008 and 2009 were investigated in this work and classified into three modes that look like some reversed formation modes (Fig. 6). The first mode is termed a reversed broken line, in which the contiguous 40-dBZ band breaks into several convective cells and each gradually dissipates (the first row in Fig. 6). The result shows that 82% of the squall lines dissipate by the reversed broken-line mode (e.g., Figs. 7a–c). The second mode is called a shrinking line in which squall lines dissipate through a contiguous shrinking of the 40-dBZ area (the second row in Fig. 6). About 11% of the cases dissipate through this mode (e.g., Figs. 7d–f). The third mode is tagged reversed broken areal, in which squall lines dissipate through the convective band turning into

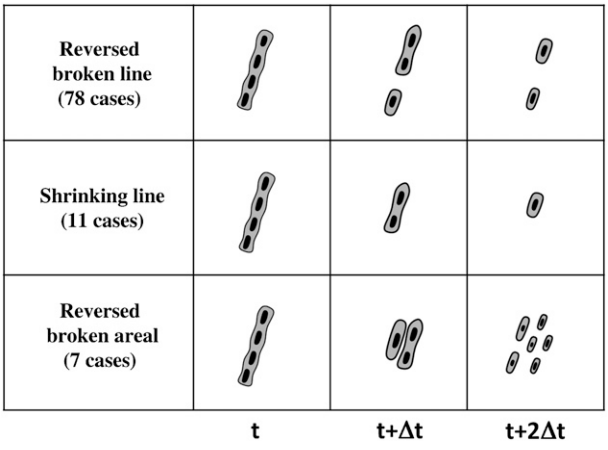

FIG. 6. The conceptual models of dissipation process of the squall lines in east China. The (top) reversed broken-line, (middle) shrinking-line, and (bottom) reversed broken-areal modes are shown.

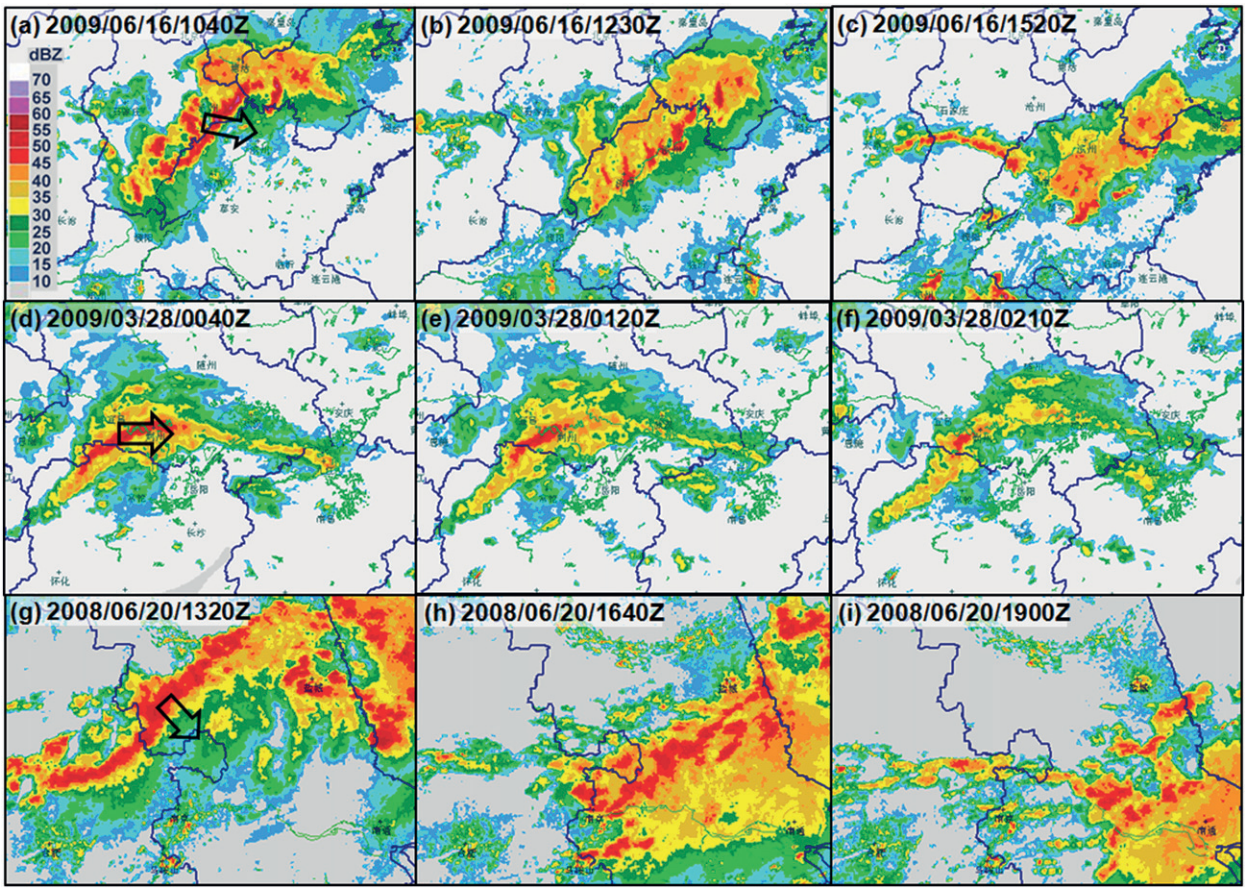

FIG. 7. Three examples of the squall lines with different dissipation modes. The open arrow in the first panel of each case denotes the direction of movement of the system during the period shown. The (a)–(c) reversed broken-line, (d)–(f) shrinking-line, and (g)–(i) reversed broken-areal modes are shown.

scattered convective cells (the third row in Fig. 6). About 7% of the cases dissipate in this mode (e.g., Figs. 7g–i). The dissipation mode of a squall line that forms in one particular mode does not necessarily dissipate in the reversed formation mode.

4. Environmental features of squall lines in east China

a. Rawinsonde composite analyses

To examine the pre-squall-line environment, a total of 19 rawinsondes that were associated with ongoing squall lines in the high-frequency areas (areas A, B, C, and D in Fig. 2a) and unaffected by local random convection were used to do the composite analyses. The following criteria are used to choose a rawinsonde that is representative of the pre-squall-line environment: the rawinsonde has to be within 300 km of the centroid of the 40-dBZ band of the squall line at the time closest to the launch time of the sounding, either passed through by the squall line or in an area that is not outside of the two lines that pass through the two ends of the 40-dBZ band pointing at 45° outward from the direction of squall line movement. Figure 8 shows the locations of the 19 rawinsondes (the filled squares with the station name and launch time in the same color) and the corresponding squall lines (the isochrones in the same color with the one closest to the launch time of the rawinsonde plotted as a heavier line). These rawinsondes were obtained from an online archive maintained by the University of Wyoming's Department of Atmospheric Science (available online at http://weather.uwyo.edu/upperair/sounding.html).

Various features from 14 out of the 19 rawinsondes that are at midlatitudes north of 30°N were used to perform composite analyses in comparison to those in the United States, subtropical areas, and preceding landfalling TCs in China. The average convective available potential energy (CAPE), convection inhibition (CIN), lifting index (LI), lifting condensation level (LCL), and precipitable water (PW) are shown in Table 3. The instability shown by CAPE and LI is smaller than that of

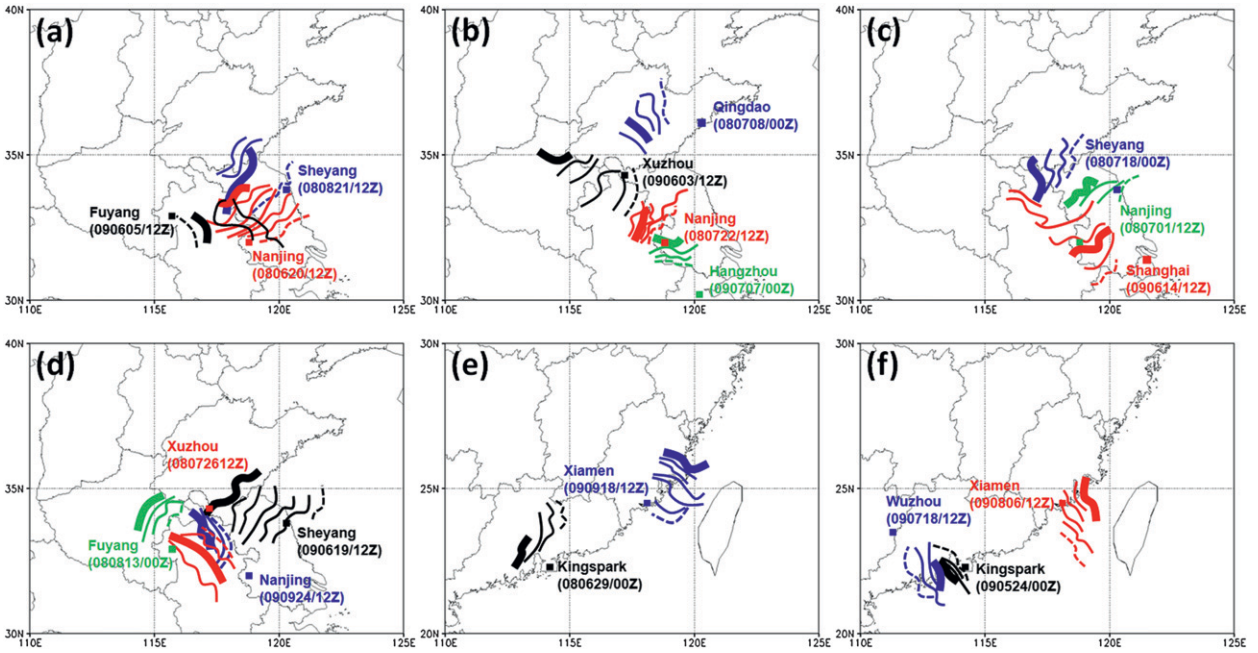

FIG. 8. The locations of the 19 soundings (filled squares, the launch times of the rawinsondes are given under the names of the rawinsonde stations) used to perform the composite analyses relative to their corresponding squall lines as shown by their isochrones (thin line, denoting the hourly leading edges of the 40-dBZ convective band) in the same color. The heavy lines denote the times that are the closest to the launch times of the rawinsondes. The dashed lines denote the ending times of the squall lines and hint at their directions of movement. Squall lines are located to the (a)–(d) north and (e),(f) south of 30°N.

the squall lines in Oklahoma (Bluestein and Jain 1985), the central United States (Parker and Johnson 2000), and preceding landfalling TCs in China (MZ12), but slightly larger than subtropical squall lines (Chen and Chou 1993) and prefrontal squall lines over the continental United States (Wyss and Emanuel 1988). The average CIN of the squall lines in midlatitude eastern China is much larger than that of the squall lines in Oklahoma (Bluestein and Jain 1985), slightly larger than that of the pre-TC squall lines, but comparable to that of the prefrontal squall lines over the continental United States (Wyss and Emanuel 1988). The average PW is slightly smaller than that of the pre-TC squall lines (MZ12) but almost twice those in the United States (Bluestein and Jain 1985; Parker and Johnson 2000), which indicates that squall lines form in a moister environment in midlatitude east China relative to the U.S. cases but in a slightly drier environment than that of the pre-TC squall lines. This sharp difference in the moisture between cases in east China and the United States is also reflected in their average LCLs with the former being 70 hPa lower than the latter.

To compare with previous studies on subtropical and pre-TC squall lines in China, the composite ground-relative winds normal and parallel to the long axis of the corresponding squall lines (the heavy lines in Fig. 9a) were determined. Facing the direction of movement of the squall line, forward is positive and backward is negative in the normal direction, while leftward is positive

TABLE 3. A comparison between the averages of the derived properties of the environmental rawinsondes of the squall lines in midlatitude east China and those in previous studies. Also given for squall lines in east China are the standard deviations (in parentheses) and the ranges of various properties.

Sounding properties		CAPE (J kg^{-1})	CIN (J kg^{-1})	LI (K)	LCL (hPa)	PW (cm)
Bluestein and Jain (1985)		2260	33			2.8
Wyss and Emanuel (1988)		1208	76			
Parker and Johnson (2000)		1605		−5.4	831	3.4
Chen and Chou (1993)		1330				
Meng and Zhang (2012)		1548	67	−3.6	899	6.1
Squall lines in east China	Avg (std dev)	1480 (644)	77 (59)	−4.3 (1.4)	909 (55)	5.6 (1.2)
at midlatitudes	Range	730 to 2583	10 to 204	−2.2 to −6.3	780 to 965	3.6 to 7

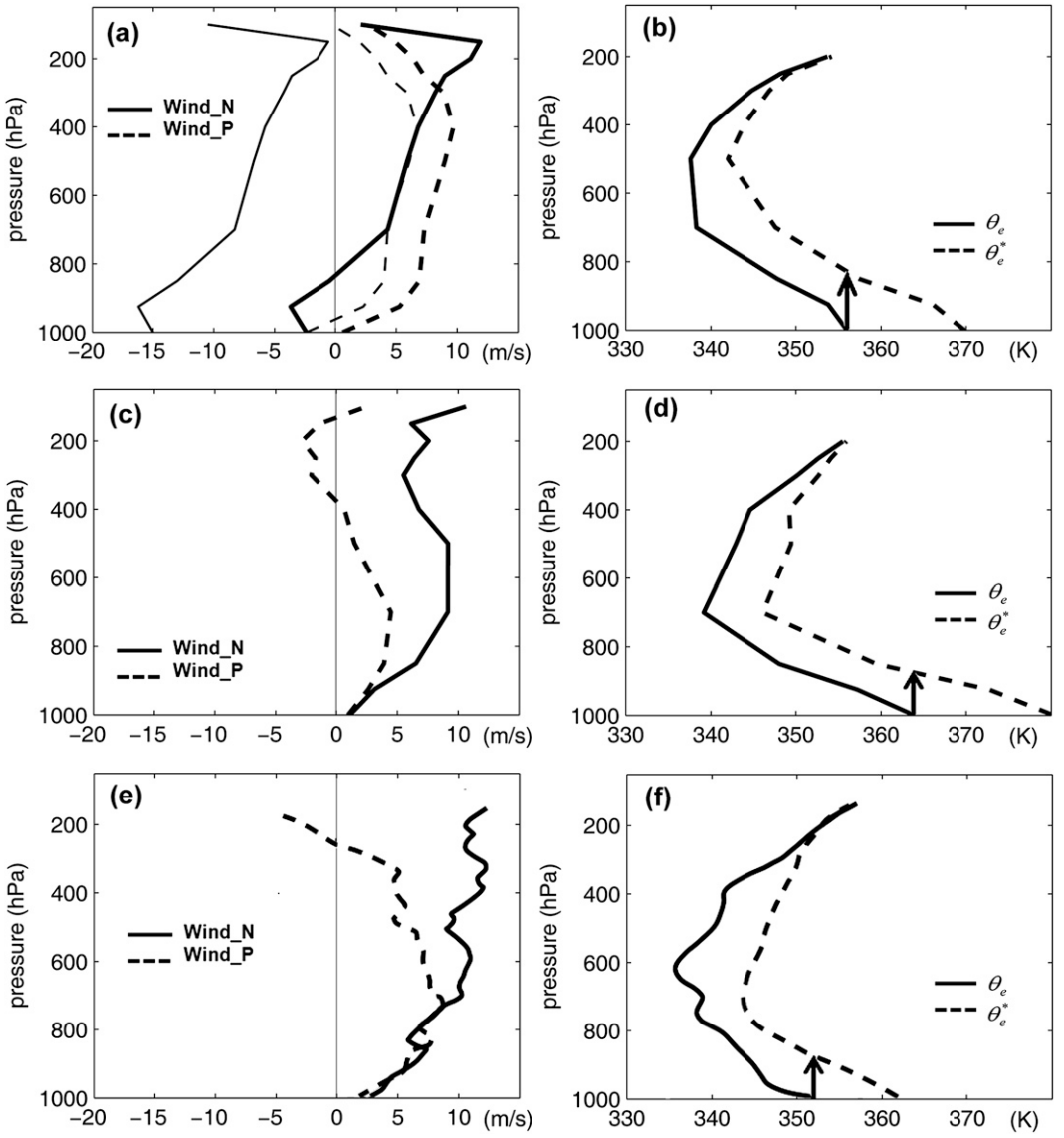

FIG. 9. (a) The composite profiles of the ground-relative (heavy lines) and line-relative (thin lines) wind components normal (Wind_N, solid) and parallel (Wind_P, dashed) to the long axis of the squall lines, and (b) the equivalent potential temperature θ_e (solid) and saturation equivalent potential temperature θ_e^* (dashed) for all 14 squall lines in the eastern China midlatitudes to the north of 30°N. The arrows in (b) indicate the rising of air parcels with surface θ_e. (c),(d) Heavy line pattern is the same as in (a),(b), but for the pre-TC squall lines (adapted from MZ12). (e),(f) Heavy line pattern is the same as in (a),(b), but for the tropical squall lines [adapted from Chen and Chou (1993)]. The gray straight lines in the left panels denote 0 m s^{-1}. The mean distance between the rawinsondes and the centroids of the corresponding squall lines is 194 km.

and rightward is negative in the parallel direction. A striking feature is the weak vertical shear and comparable line-normal and line-parallel low-level vertical shear. The 1000–500-hPa (approximately 0–6 km) line-normal vertical wind shear is about 9 m s^{-1}. It is slightly larger than the 1000–500-hPa line-parallel vertical wind shear. This feature is apparently different from pre-TC squall lines where an apparently larger 1000–500-hPa line-normal relative to line-parallel vertical shear was observed (Fig. 9c, adapted from MZ12), fast-moving tropical squall lines (e.g., Barnes and Sieckman 1984), and subtropical (Fig. 9e, adapted from Chen and Chou 1993) and midlatitude (e.g., Bluestein and Jain 1985; Wyss and Emanuel 1988) squall lines. The 1000–700-hPa line-normal vertical shear in midlatitude east China is also close to the line-parallel component, which is similar to that in

Chen and Chou (1993) (Fig. 9e). The line-relative wind profiles normal and parallel to the squall lines in midlatitude east China are plotted as thin lines in Fig. 9a. The result shows that the storm-relative line-normal wind component is negative at all levels with the strongest wind around 925 hPa. The storm-relative line-parallel mean wind is much weaker than the line-normal component at low levels.

The mean equivalent and saturation equivalent potential temperature [$\theta_e^* = \theta \exp(Lq_{vs}/c_pT)$, where L is the latent heat of vaporization, q_{vs} is the saturation mixing ratio, c_p is the specific heat of dry air at constant pressure, and T is the air temperature (Houze 1993, p. 54)] show that the squall lines in midlatitude east China have a deeper layer of conditional instability (θ_e^* decreases with height; Fig. 9b) and a higher level of free convection (LFC, the cross point between the constant surface θ_e and θ_e^* as indicated by the head of the arrow) than that of the pre-TC squall lines in China (Fig. 9d, adapted from MZ12) and the subtropical squall lines [Fig. 9f, adapted from Chen and Chou (1993)], which is consistent with their larger CINs. The area enclosed by the straight line (parallel to the y axis crossing the x axis at the equivalent potential temperature at 1000 hPa) and the saturation equivalent potential temperature for the squall lines in midlatitude east China (Fig. 9b) is smaller than that of the pre-TC squall lines (Fig. 9d), which is consistent with its smaller CAPE (Table 3). Both the squall lines in midlatitude east China and the pre-TC squall lines in China have larger instability than that of the subtropical squall lines [Fig. 9f, adapted from Chen and Chou (1993)].

To provide a general picture of the possible differences in the environments of squall lines with different formation and organization modes and to see if there are any consistencies between them and their U.S. counterparts, a total of 19 rawinsondes were classified in terms of their formation and organizational modes. It is important to keep in mind that due to the limited number of samples, the results of this subclassification process may not be completely generalizable.

Concerning the formation modes, the BB cases have the largest CAPE, smallest CIN, smallest LI, lowest LCL and LFC (Figs. 10b,d,f,h), and largest precipitable water (Table 4). This is different from the results of Bluestein and Jain (1985) in which the BL cases have the largest CAPE and smallest CIN. The BL cases form in the driest environment with the least PW, largest CIN, and highest LFC. The EA cases exhibit the smallest CAPE and largest LI, indicating that the EA cases tend to form in a more stable environment, which is consistent with the results for squall lines in Oklahoma (Bluestein and Jain 1985) and MCSs in the central United States (Jirak et al. 2003). The main differences in the line-relative wind features among different modes lie in the line-normal wind component at all levels and the line-parallel wind component at the upper levels (Figs. 10a,c,e,g). Both the BL and BA cases have negative line-normal wind components at all levels. The BL, BB, and EA cases have large high-level line-parallel flow, which may help to advect hydrometers along the line, thus favoring the linear growth of the squall lines. The negative high-level line-parallel flow of the BB cases may help to advect hydrometers to the right of the squall-line movement where new convection is usually triggered (Abdullah 1954). The BL and BA cases have larger line-parallel than line-normal vertical wind shears of both 1000–500 and 1000–700 hPa (Fig. 10). The BA cases have the largest line-parallel vertical wind shear of 1000–500 hPa. The BB and EA types have apparently larger line-normal vertical wind shears of both 1000–500 and 1000–700 hPa. Another interesting feature is that there are apparently large high-level line-parallel vertical wind shears of around 15 m s^{-1} between 500 and 200 hPa in the BA, BB, and EA cases, which may be helpful in the linear growth of convection (Grady and Verlinde 1997).

From the organizational-mode point of view, the LS cases are apparently different from the TS and PS classes. They have the largest CAPE, smallest CIN, lowest LCL and LFC (Figs. 11b,d,f), and highest precipitable water (Table 4). This result is different than that for squall lines in the central United States (Parker and Johnson 2000), where the TS cases have the largest CAPE, lowest LCL, and largest PW. The LS cases also have the most apparent dominating line-normal vertical wind shear for both 1000–500 and 1000–700 hPa relative to the line-parallel components (Fig. 11). Furthermore, the LS and PS cases have apparently dominant low-level line-normal wind shear relative to the TS cases. The mean wind profiles exhibit the most apparent differences among the different cases at high levels (Figs. 11a,c,e). The LS cases have the largest upper-level rear-to-front line-relative flow, which advects hydrometers forward to form the leading stratiform precipitation. The TS cases exhibit negative line-normal storm-relative wind at all levels with the largest magnitude among the three modes, especially, found at high levels (Fig. 11a). This flow advects hydrometers rearward and results in the trailing stratiform precipitation (e.g., Rutledge 1986). The PS cases exhibit an apparently larger line-parallel wind component than the line-normal component around 200 hPa, which may have helped to advect hydrometers along the squall lines. These features are consistent with the results of squall lines in the central United States (Parker and Johnson 2000).

b. Environmental flow patterns

To further examine the environment favorable for the formation of squall lines in east China, the synoptic

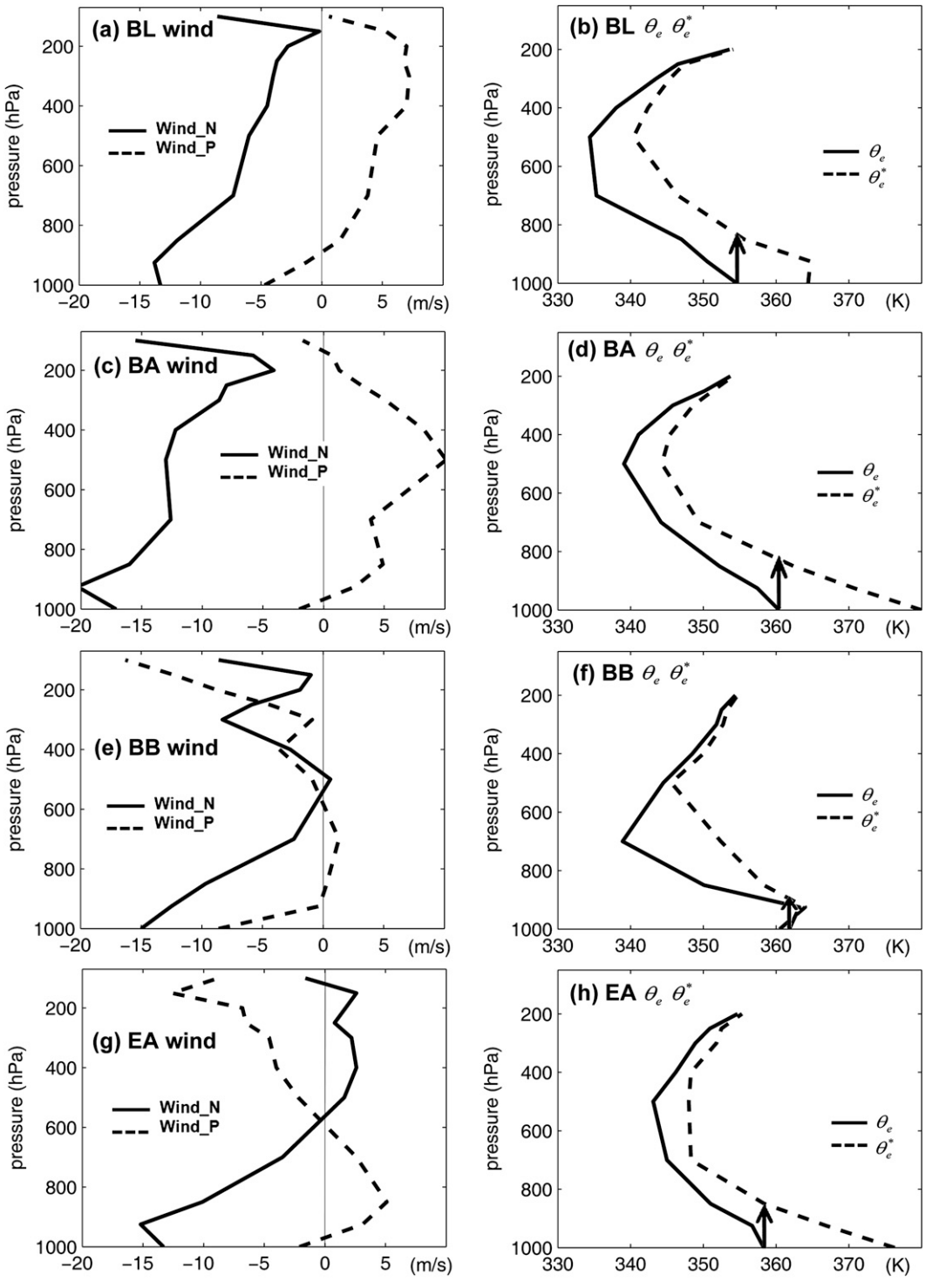

FIG. 10. (left) The composite profiles of the wind component normal (solid) and parallel (dashed) to the long axis of the squall lines and (right) the equivalent potential temperature θ_e (solid) and saturation equivalent potential temperature θ_e^* (dashed) for the squall lines with different formation modes: (a),(b) broken line; (c),(d) broken areal; (e),(f) back building; and (g),(h) embedded areal. The arrows in the right panels indicate the rising of air parcels with surface θ_e. The gray straight lines in the left panels denote 0 m s^{-1}. The mean distances between the rawinsondes and the centroids of the corresponding squall lines for the BL, BA, EA, and BB formation modes are 225, 163, 180, and 204 km, respectively.

TABLE 4. A comparison between the averages, standard deviations (in parentheses), and ranges (in the second line of each category) of the derived properties of the environmental rawinsondes of the squall lines in east China among different formation and organizational modes. The numbers of squall lines of different types are given in the parentheses in the first column. Since only two samples are identified for the BB pattern, its standard deviation was not calculated.

Sounding properties	CAPE (J kg^{-1})	CIN (J kg^{-1})	LI (K)	LCL (hPa)	PW (cm)
BL (7)	1432 (580)	94 (58)	−4.3 (1.3)	915 (55)	5.2 (1.3)
	858 to 2307	26 to 204	−6 to −2.7	799 to 965	3.6 to 7
BB (2)	1933	25	−4.9	954	6.3
	1282 to 2583	11 to 40	−6.2 to −3.7	954.2 to 954.3	6.2 to 6.3
BA (6)	1866 (110)	67 (62)	−4.5 (1.5)	895 (61)	6.0 (1.1)
	932 to 3808	15 to 156	−6.3 to −2.6	780 to 942	3.8 to 6.9
EA (4)	1149 (384)	48 (55)	−2.7 (0.7)	903 (55)	6.2 (0.6)
	730 to 1657	5 to 123	−3.7 to −2.2	822 to 941	5.6 to 7
TS (10)	1706 (897)	75 (68)	−4.7 (1.3)	901 (63)	5.5 (1.3)
	932 to 3808	11 to 204	−6.3 to −2.6	780 to 954	3.6 to 6.9
LS (4)	1819 (823)	32 (18)	−3.9 (1.8)	928 (21)	6.5 (0.7)
	730 to 2583	10 to 53	−6.2 to −2.2	907 to 954	5.6 to 7
PS (5)	1068 (133)	84 (46)	−3.0 (0.6)	915 (55)	5.8 (0.8)
	858 to 1206	5 to 123	−3.7 to −2.3	822 to 965	4.7 to 6.7

features of the 45 squall lines in the four high-frequency areas (8 from A, 29 from B, 4 from C, and 4 from D) were analyzed using the 6-hourly final analyses (FNL) of the National Centers for Environmental Prediction (NCEP) 1° × 1° gridded data (available online at http://dss.ucar.edu/datasets/ds083.2). The environmental flows of 44 out of the 45 squall lines can be categorized into six patterns including pre–short trough, pre–long trough, cold vortex, subtropical high, TC, and posttrough (Fig. 12) largely by identifying their dominant ambient weather systems. One case cannot be grouped into any of the six patterns.

The pre-short-trough pattern is most common, accounting for about one-third of the 45 squall lines. This pattern features a short trough (the trough base line spans shorter than 1000 km) in a zonal flow in northern China that is usually to the north of 30°N with the subtropical high to its southeast (e.g., Figs. 12a,b). The adequate moisture supply through the southeasterly flow on the west edge of the subtropical high seems to play an important role in the formation of the squall lines in this pattern. The moisture supply may become more favorable when a TC makes landfall as in the predecessor rainfall events (PREs, the heavy rains occur far from the landfalling TC due to the distant transportation of moisture from the TC area; Galarneau et al. 2010; Dong et al. 2010; Schumacher et al. 2011; Schumacher and Galarneau 2012).

The pre-long-trough pattern is characterized by more longitudinal flow (e.g., Figs. 12c,d). The base of the trough usually spans more than 1500 km and extends to the south of 30°N. This pattern is associated with rich moisture, a low-level jet, and moderate (10–20 m s^{-1}) 1000–700-hPa vertical shear.

The cold-vortex pattern features an extensive and quasi-stationary cyclonic vortex in northeast China (e.g., Figs. 12e,f). Cold vortices are slow-moving cold-core cyclonic centers in the mid- to upper troposphere. Squall lines commonly form in front of a west–east-oriented short trough embedded in the west half of the cold vortices when the short trough propagates to the south or southeast. Favorable conditions are likely to be unstable environments due to the overlaying of cold air on top of warm air together with short-wave disturbances. The air is drier relative to other patterns and no apparent low-level jet is observed in this pattern.

Another pattern is characterized by the Pacific subtropical high immediately neighboring the continental high (e.g., Figs. 12g,h). Squall lines are mainly initiated on the western flank of the Pacific subtropical high north of an embedded west–east-oriented 850-hPa short-wave trough. Squall lines of this pattern form basically in an environment with weaker high-level forcing for ascent but benefit likely from rich moisture transported by northward flows, shortwave disturbances, and moderate 1000–700-hPa vertical shear (about 10 m s^{-1}).

As shown in MZ12, squall lines may also form near a TC mainly in the transition area between the TC and the neighboring subtropical high (white dots in Figs. 12a,b). The parent TC may help convective initiation through enhancing the moisture, conditional instability, and low-level convergence and consequently linear organization of the squall line (MZ12).

Squall lines may also form behind an upper-level trough and in front of a lower-level trough. We have only one sample in this pattern. This result is different from the results of Ding et al. (1982), who showed that posttrough is a dominant environmental flow pattern of squall lines in

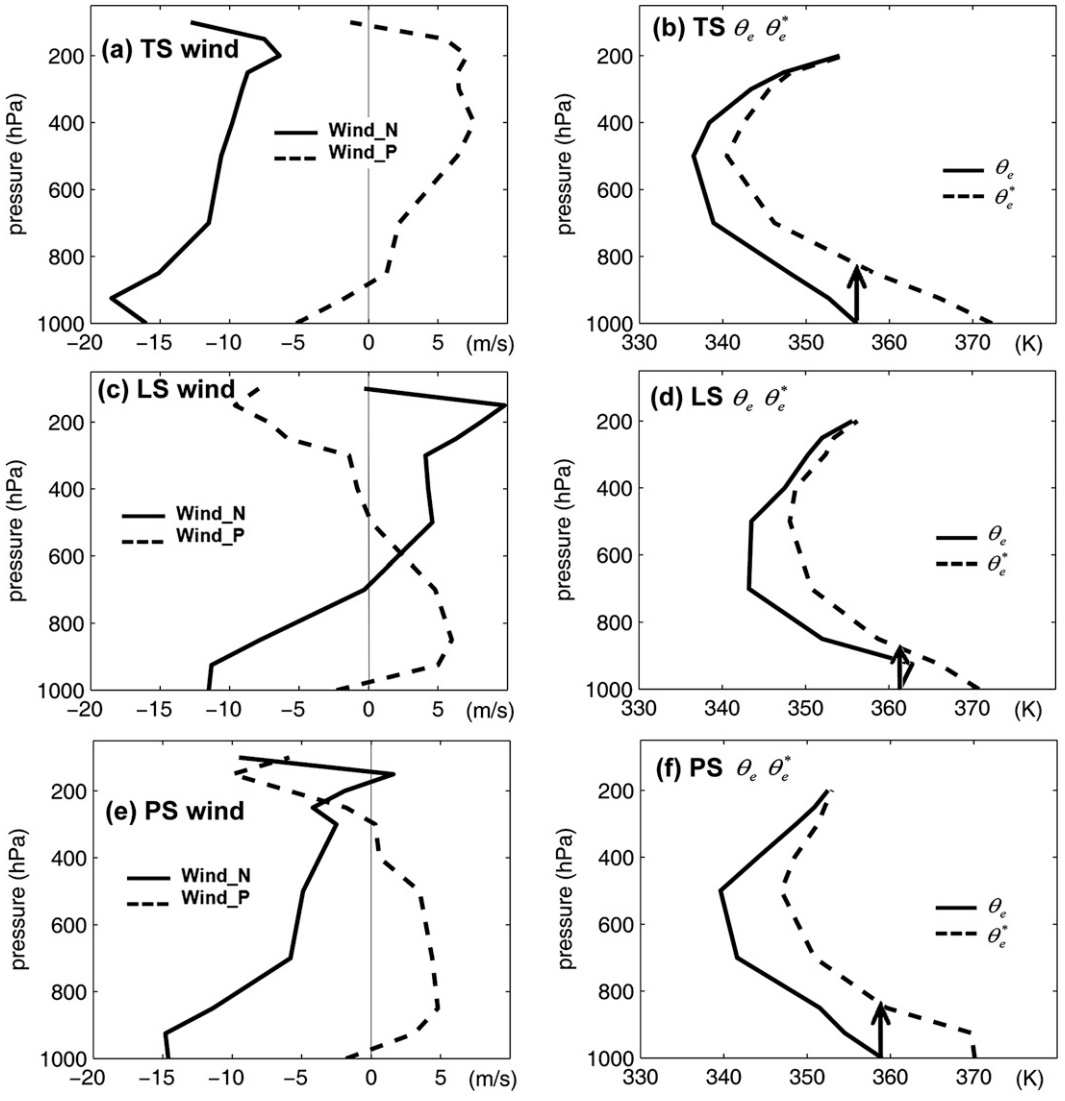

FIG. 11. As in Fig. 10, but for organizational modes: (a),(b) TS; (c),(d) LS; and (e),(f) PS. The mean distances between the rawinsondes and the centroids of the corresponding squall lines for the TS, LS, and PS modes are 186, 200, and 204 km, respectively.

north China. The reasons behind this difference may have their roots in the following causes. 1) The subjective definitions used when classifying the weather patterns. 2) The data used to analyze the patterns are different in both spatial and temporal resolutions. Ding et al. (1982) used manual analyses based on conventional rawinsondes while this work uses the NCEP global analyses. 3) The criteria used to identify a squall line are different. This work determines a squall line using radar reflectivity features, while Ding et al. (1982) determined a squall line likely based on the features of surface observational variables though they did not mention how exactly they defined a squall line. 4) The target area is different. The present work focuses on a much larger area of the whole eastern China region than did Ding et al. (1982), who examined only the squall lines in north China and Hunan Province.

5. Sensitivity of squall-line features to different criteria

As mentioned by Geerts (1998), a slight increase in lower reflectivity thresholds in the squall-line determination scheme may rapidly trim the database, which suggests that there is a fairly distinct tail in the distribution of reflectivity values in MCSs. This feature is confirmed in our study.

The statistical results in previous sections were obtained using the criteria that require a strictly contiguous

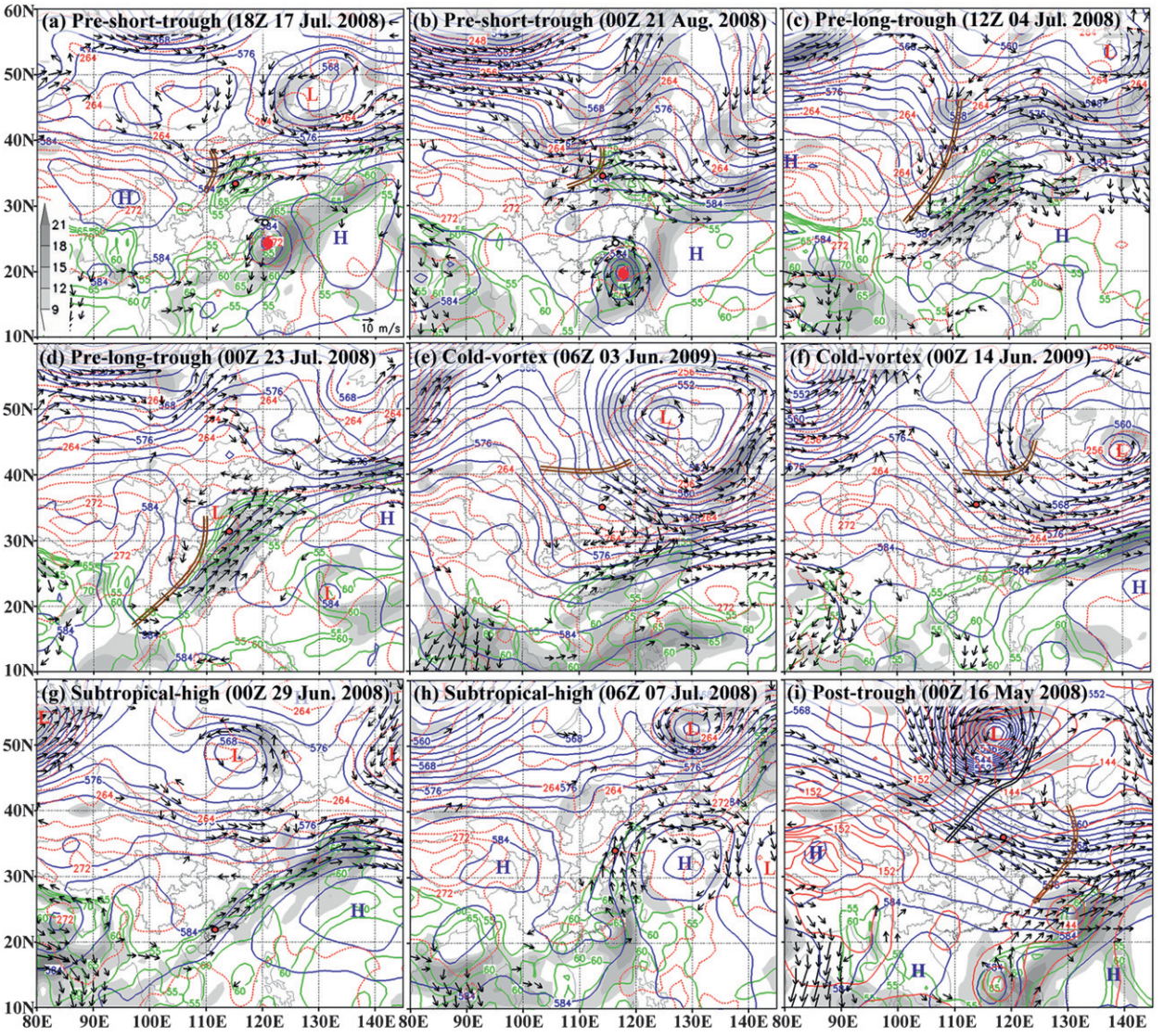

FIG. 12. Examples of various environmental flow patterns at (a) 1800 UTC 17 Jul 2008 and (b) 0000 UTC 21 Aug 2008 for pre-short-trough cases, (c) 1200 UTC 4 Jul 2008 and (d) 0000 UTC 23 Jul 2008 for pre-long-trough cases, (e) 0600 UTC 3 Jun 2009 and (f) 0000 UTC 14 Jun 2009 for cold-vortex cases, (g) 0000 UTC 29 Jun 2008 and (h) 0600 UTC 7 Jul 2008 for subtropical-high cases, and (i) 0000 UTC 16 May 2008 for posttrough cases. Plotted are geopotential height [blue contours, 10 geopotential meters (gpm)], temperature (dashed red contours, K) at 500 hPa, column-integrated PW greater than 55 kg m^{-2} (green contours, kg m^{-2}), vertical shear vector between 700 and 1000 hPa with the magnitude larger than 8 m s^{-1} [the representative wind vector is given in the bottom-right corner of (a)], and wind speed larger than 9 m s^{-1} at 850 hPa (shaded, every 3 m s^{-1}). The double solid brown lines denote the trough at 500 hPa. The red solid contour and the double solid black lines in (i), respectively, denote the geopotential height (10 gpm) and the trough at 850 hPa. The places where the convection of the squall line was initiated are marked by red dots. The white dots indicate the areas that also have a possibility of squall-line formation near a TC. Here, H and L denote the high and low pressure centers at 500 hPa, respectively. The TC centers are given by the red typhoon marks in (a) and (b).

100-km-long 40-dBZ rainband last for at least 3 h (referred to as criteria 1). When the criteria are changed into a quasi-contiguous 100-km-long 40-dBZ rainband that lasts at least 3 h with a strictly contiguous 100-km-long 45-dBZ rainband appearing sometime during the life span of the squall line (referred to as criteria 2), the number of identified squall lines is almost tripled. A comparison was performed between the samples obtained with the two sets of criteria for the year 2008. With criteria 1, 52 squall lines were identified in 2008, while 141 squall lines were obtained using the new weaker criteria 2.

Though the number of the squall lines is substantially increased, the spatial and temporal distributions still show similar features. The largest frequency of formation also

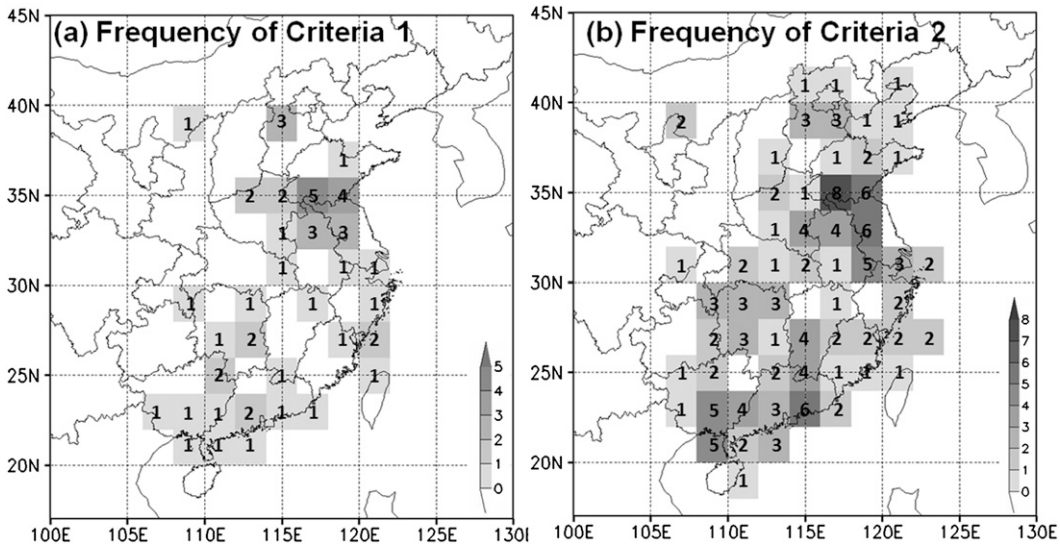

FIG. 13. The geographical distribution of the squall-line formation (shaded) in east China during 2008 with (a) criteria 1, which requires a strictly contiguous 40-dBZ band, and (b) criteria 2 which allows a quasi-contiguous 40-dBZ band. The exact number of the frequency of the squall-line formation is given in the grid box.

appears in the boundary area around Jiangsu, Shandong, Henan, and Anhui Provinces (Fig. 13), with minor high-frequency areas in Hebei, Fujian, and Guangdong provinces. The seasonal variation also peaks in July (Fig. 14a). The three diurnal peaks under criteria 1 turn into a major peak during 1200–1500 LST and a minor peak during 0300–0600 LST (Fig. 14b).

Radar signatures also take on similar frequency distributions. The maximum length, maximum intensity, life span, and speed of movement all peak in the same value range, though with larger tails (Figs. 14c–f). The maximum length increases from 400 to 600 km, consequently the average maximum length increases from 230 to 253 km. The average maximum intensity decreases due to the weaker criteria from 58–63 to 57–62 dBZ. The average life span also increases from 4.6 to 5 h. The weaker criteria result in a smaller average speed of movement of 12.8 m s^{-1} relative to the former 14.2 m s^{-1}. Since the weaker criteria are close to that used by MZ12 in their statistics of the pre-TC squall lines, the smaller speed of movement is close to that of the pre-TC squall line of 12.5 m s^{-1}.

The dominant modes of squall-line formation, organization, and dissipation are still the same as those obtained with the stronger criteria, namely a dominant broken-line formation, a trailing-stratiform pattern, and a reversed broken-line dissipation mode.

6. Summary

Using composite radar reflectivity mosaics from east China during 2008 and 2009, this work has investigated the general features of squall lines and may provide important references for real-time forecasts. The criterion used to identify a squall line is that a linear or quasi-linear contiguous 40-dBZ band of no shorter than 100 km lasts at least 3 h.

This survey identified 96 squall lines with maximum frequencies of occurrence in north China near the boundaries between Shandong, Henan, Anhui, and Jiangsu Provinces. Three secondary maxima in the frequency of occurrence are located in Hebei, Guangdong, and Fujian Provinces. The squall lines range from March to October with a peak in July. The formation zone shifts from south in spring to north in summer and then goes back to the south in autumn. This month-to-month shift of the squall-line formation may be associated with the shift of the baroclinic zone between the subtropics and extratropics.

The diurnal variation shows a major peak in the early evening and two minor peaks in the early morning and early afternoon. The early evening peak is not sensitive to the latitudes where the squall lines form while the other two minor peaks are. The early morning peak is mostly attributed to the squall lines that form to the south of 30°N, while the early afternoon peak is mostly attributed to the squall lines that form to the north of 30°N, both of which are likely due to the corresponding peaks of the appearances of their first echoes. The time between the formation of the squall lines and the appearance of their first echoes is about 4.8 h and is not sensitive to their latitudinal locations.

The squall lines have a dominant southwest–northeast orientation, an eastward motion at a speed of 14.4 m s^{-1},

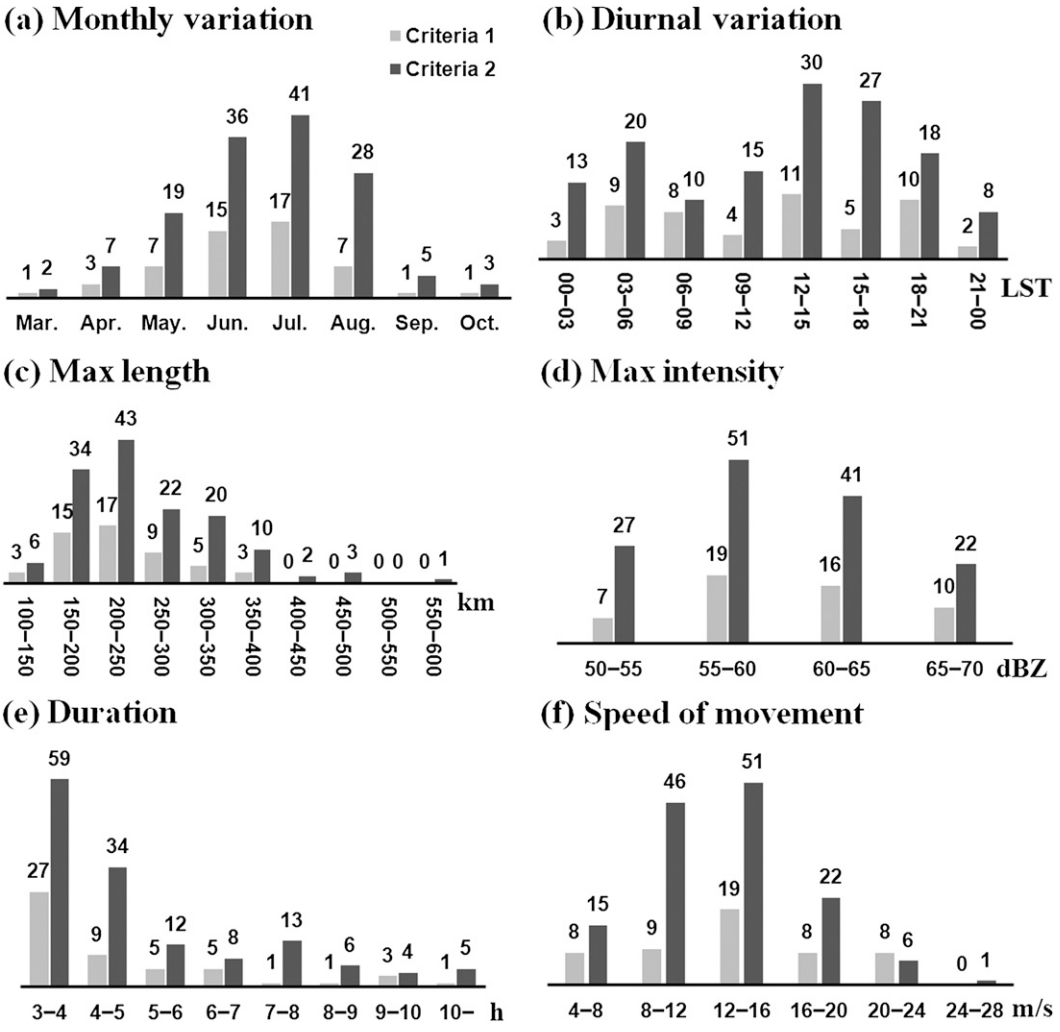

FIG. 14. The frequency of formation of the squall lines in 2008 with respect to various radar traits including (a) monthly variation, (b) diurnal variation, (c) the maximum length, (d) the maximum intensity in terms of the composite radar reflectivity, (e) duration, and (f) speed of movement based on the two different criteria. The light gray bars denote the squall lines with criteria 1, which requires a strictly contiguous 40-dBZ band, while the dark gray bars denote the squall lines with criteria 2, which allows a quasi-contiguous 40-dBZ band.

a maximum length of 243 km, a maximum intensity of 58–63 dBZ, and a duration of 4.7 h on average. The squall lines commonly form in the broken-line mode, take on the trailing-stratiform pattern, and dissipate in the reversed broken-line mode. Relative to the U.S. cases, squall lines in east China tend to have more cases that form in an embedded-areal pattern.

The preline rawinsondes in the area with high frequency of formation were composited. Results show that squall lines in midlatitude eastern China form in a moister environment with comparable background instability, and weaker vertical shear relative to their U.S. counterparts. The line-normal vertical wind shear is comparable to the line-parallel component. The line-normal flow is rearward and stronger than the line-parallel components at all levels on average. The composite rawinsonde features were also examined for different formation and organizational modes. An apparent difference is that the largest instability and the most humid environment are observed in the squall lines with a leading stratiform in eastern China rather than with trailing stratiform in the U.S. situation. The largest difference among different organizational modes lies in high-level flows especially the line-normal winds, which exhibit some similarity to the features of squall lines in the United States.

The environmental flows of the squall lines in the area with high frequency of formation were summarized into six background synoptic weather patterns: pre–short trough, pre–long trough, cold vortex, subtropical high,

TC, and posttrough. About one-third of the squall lines in east China form in the pre-short-trough pattern. The posttrough pattern has the fewest squall lines. Favorable conditions of various patterns were examined. The pre-short-trough pattern features adequate moisture supply. The pre-long-trough pattern is associated with rich moisture, a low-level jet, and moderate 1000–700-hPa vertical shear. The cold-vortex and posttrough patterns have favorable environmental instability. The subtropical-high pattern is characteristic of rich moisture transported by southerly flows, short-wave disturbances, and moderate 1000–700-hPa vertical shear. The TC pattern has rich moisture, high conditional instability, and low-level convergence.

This work provided only a basic description of the squall-line climatology in eastern China based on a 2-yr period of radar data. Additional years of data will be used when available in future work to bolster and potentially expand upon the conclusions of the current study. Further efforts will also be made to explore convective initiation mechanisms in the high moist and low vertical shear climate regime through more in-depth observational analyses and cloud-resolving numerical simulations of typical cases of various flow patterns.

Acknowledgments. We thank Fuqing Zhang from The Pennsylvania State University for his constructive comments. The radar mosaics were made available by the Chinese National Meteorological Center. This research is sponsored by Grants 2013CB430104, NSFC41075031, NSFC40921160380, and GYHY201306004.

REFERENCES

Abdullah, A. J., 1954: The meridional growth of squall lines. *J. Meteor.,* **11,** 301–308.

Bao, X., F. Zhang, and J. Sun, 2011: Diurnal variations of warm-season precipitation east of the Tibetan Plateau over China. *Mon. Wea. Rev.,* **139,** 2790–2810.

Barnes, G. M., and K. Sieckman, 1984: The environment of fast- and slow-moving tropical mesoscale convective cloud lines. *Mon. Wea. Rev.,* **112,** 1782–1794.

Bluestein, H. B., and M. H. Jain, 1985: Formation of mesoscale lines of precipitation: Severe squall lines in Oklahoma during the spring. *J. Atmos. Sci.,* **42,** 1711–1732.

Chen, G. T.-J., and H.-C. Chou, 1993: General characteristics of squall lines observed in TAMEX. *Mon. Wea. Rev.,* **121,** 726–733.

Ding, Y.-H., H.-Z. Li, M.-L. Zhang, J.-S. Li, and Z.-Y. Cai, 1982: A study on the formation condition of squall line in China (in Chinese). *Chin. J. Atmos. Sci.,* **6,** 18–27.

Dong, M., L. Chen, Y. Li, and C. Lu, 2010: Rainfall reinforcement associated with landfalling tropical cyclones. *J. Atmos. Sci.,* **67,** 3541–3558.

Galarneau, T. J., Jr., L. F. Bosart, and R. S. Schumacher, 2010: Predecessor rain events ahead of tropical cyclones. *Mon. Wea. Rev.,* **138,** 3272–3297.

Geerts, B., 1998: Mesoscale convective systems in the southeast United States during 1994–95: A survey. *Wea. Forecasting,* **13,** 860–869.

Glickman, T. S., Ed., 2000: *Glossary of Meteorology*. 2nd ed. Amer. Meteor. Soc., 855 pp.

Grady, R. L., and J. Verlinde, 1997: Triple-Doppler analysis of a discretely propagating, long-lived, high plains squall line. *J. Atmos. Sci.,* **54,** 2729–2748.

He, H., and F. Zhang, 2010: Diurnal variations of warm-season precipitation over northern China. *Mon. Wea. Rev.,* **138,** 1017–1025.

Houze, R. A., Jr., 1993: *Cloud Dynamics.* Academic Press, 573 pp.

——, B. F. Smull, and P. Dodge, 1990: Mesoscale organization of springtime rainstorms in Oklahoma. *Mon. Wea. Rev.,* **118,** 613–654.

Jirak, I. L., W. R. Cotton, and R. L. McAnelly, 2003: Satellite and radar survey of mesoscale convective system development. *Mon. Wea. Rev.,* **131,** 2428–2449.

Meng, Z., and Y. Zhang, 2012: On the squall lines preceding landfalling tropical cyclones in China. *Mon. Wea. Rev.,* **140,** 445–470.

Parker, M. D., and R. H. Johnson, 2000: Organizational modes of midlatitude mesoscale convective systems. *Mon. Wea. Rev.,* **128,** 3413–3436.

Rotunno, R., J. B. Klemp, and M. L. Weisman, 1988: A theory for strong, long-lived squall lines. *J. Atmos. Sci.,* **45,** 463–485.

Rutledge, S. A., 1986: Diagnostic modeling study of the stratiform region associated with a tropical squall line. *J. Atmos. Sci.,* **43,** 1356–1377.

Schumacher, R. S., and T. J. Galarneau Jr., 2012: Moisture transport into midlatitudes ahead of recurving tropical cyclones and its relevance in two predecessor rain events. *Mon. Wea. Rev.,* **140,** 1810–1827.

——, ——, and L. F. Bosart, 2011: Distant effects of a recurving tropical cyclone on rainfall in a midlatitude convective system: A high-impact predecessor rain event. *Mon. Wea. Rev.,* **139,** 650–667.

Wyss, J., and K. A. Emanuel, 1988: The pre-storm environment of midlatitude prefrontal squall lines. *Mon. Wea. Rev.,* **116,** 790–794.

Zhang, Y., Z. Ding, and X. Huang, 2012: Analysis on formation reason of a squall line weather in the Yellow River and Huaihe River basins (in Chinese). *J. Anhui Agric. Sci.,* **40,** 10 981–10 983.

Zhu, X., and J. Zhu, 2004: New generation weather radar network in China (in Chinese). *Meteor. Sci. Technol.,* **32,** 255–258.